

Development and Application of GPS Signal Multipath Simulator

Sung H. Byun, George A. Hajj, and Lawrence E. Young

Jet Propulsion Laboratory, California Institute of Technology, Pasadena, California, USA

Abstract. A ray tracing GPS signal multipath simulator which takes into account the signal reflection and diffraction from surrounding objects has been developed. By properly modeling the environment around an antenna and the GPS receiver's tracking loop, this simulator can assess the GPS signal multipath error. Thus, it can be used in the early design phase of an experiment to foretell hazardous environmental configurations that can cause severe multipath. It can also aid in finding the best antenna type, location, and orientation within a given environment, and provides a quantitative estimate of multipath errors on GPS measurements. The capability of the simulator is demonstrated by using the International Space Station (ISS) environment.

1. Introduction

The Global Positioning System (GPS), consisting of a minimum of 24 satellites evenly distributed in six orbital planes at 20200 *km* altitude, has been shown to be capable of supporting a wide variety of applications. Current baseline solutions accuracies using the GPS is 1-2 parts in 10^9 , while those of orbit positioning are of the order of few parts in 10^9 . A wide range of techniques have been developed over the past fifteen years that must be used in order to achieve such accuracies. Some of these techniques pertain to better modeling of forces acting on the GPS or a user's satellite and on ground stations; while others pertain to improved range and phase data. Data accuracies are limited by instrumental thermal noise, tropospheric effects, higher order ionospheric effects, and multipath. Advanced receiver's instrumental noise is now reaching an RMS of 10 *cm* for range (P-code) and 0.1 *mm* for range-rate (phase) after one second averaging. The tropospheric effect can be modeled to the *cm* level while higher order ionospheric effects, under normal conditions, are expected to be less than 1 *cm* [Bassiri and Hajj, 1993].

Differential GPS can greatly reduce common er-

Copyright 2002 by the American Geophysical Union.

Paper number .
0048-6604/02/\$11.00

rors resulting from atmospheric delay, GPS orbit, and GPS and/or receiver clocks. However, the GPS multipath errors can not be removed by differential approach since multipath is a highly localized phenomenon. Thus, one of the major error contributors to GPS positioning application can be multipath.

Multipath is the phenomenon where a signal arrives at an antenna via several paths due to signal reflection and diffraction. Its sources can be the transmitting or the receiving antenna environment. Multipath error is scaled according to wavelength and is generally therefore nearly 100 times larger for P-code than carrier phase. Instantaneous multipath error can be as large as few meters for P-code and few centimeters for carrier phase. Thus, in situations where instantaneous range and phase data, or data averaged over small time intervals are needed, multipath becomes a dominant source of error to the measurement.

In addition to contributing to positioning error, multipath can cause serious problems on a host of other GPS derived applications. Examples are gravity recovery and atmospheric occultation. In the former, multipath errors that are not averaged over the period of the experiment will be directly mapped in the spherical harmonics; while in the latter, where instantaneous phase data are needed, multipath error will be mapped into the recovered atmospheric refractivity.

In this paper, the multipath effect on the GPS signal and its implications on orbit and ground positioning are examined. In order to do this, a multipath simulator, MUSTARD (MULTipath Simulator Taking into Account Reflection and Diffraction), has been developed. The following sections will describe the theoretical background and the application of the simulator.

1.1. Multipath Problem

If a satellite's signal propagates along a direct path to the receiver's antenna, the receiver can accurately determine the satellite range. However, the GPS signal can be easily reflected by other objects, thus resulting in possibly multiple secondary paths as shown in figure 1. These paths are always longer than the direct path, and are superimposed on the direct signal at the antenna with a different phase and amplitude. The signal wave-form's amplitude and phase can be significantly distorted by these secondary paths and thus can result in significant ranging errors. We distinguish between multipath due

to structures in the propagation media (ionosphere, stratosphere, and troposphere) and multipath due to objects near the transmitter and receiver. It is only the latter case that concerns us in this study.

1.2. Previous Work

In this section, some of the important previous work regarding multipath mitigation is reviewed. There are two main approaches in dealing with the multipath problem: signal processing within the GPS receiver, and multipath mitigation performed outside the receiver. Recently, important progress has been made in GPS receiver technology [Weill, 1997; Meehan and Young, 1992]. However, only multipath mitigation techniques performed outside the receiver—the multipath simulator is one of them—are reviewed in this article. These methods try to preserve the direct-path signal while reducing the multipath signal.

1.2.1. Special antennas.

1.2.1.1. Antenna gain pattern: In practice, antennas do not receive signals equally from all directions. By properly shaping an antenna gain pattern, partial signal rejection can be built into it. In surveying, for example, multipath can be reduced by shaping the antenna to have low gain in near horizontal directions since most multipaths arrive from that angles [Schupler *et al.*, 1994; Stutzman and Thiele, 1997]. However, specialized shaping of the gain pattern may require an antenna array, large antenna aperture, or other demanding manufacturing process. This might be acceptable for the ground stations in surveying but may not be suitable for highly dynamic applications where compact antennas size and omni-directional antenna gain are desired.

1.2.1.2. Antenna polarization: The antenna polarization can provide additional multipath attenuation. The direct GPS signal received at the antenna is right-hand circularly polarized (RCP). In theory, a RCP signal becomes left-hand circularly polarized (LCP) upon reflection from an ideal conducting object, and an LCP signal would be completely rejected by an ideal GPS antenna. Unfortunately, total LCP signal rejection is not obtained in reality but a GPS antenna designed for the RCP GPS signals is not nearly as sensitive to the LCP signal and, thus, provides some degree of attenuation to multipath signals from reflection.

1.2.1.3. Choke-ring antenna: The multipath error can be reduced by placing radio-frequency ab-

sorbing material underneath the antenna, thus improving the antenna gain pattern characteristics. This led to the notion of using a horizontal metallic disk at the base of GPS antenna so that the extended ground-plane would shield the antenna from any multipath from below. When a multipath signal from below arrives at the edge of the disk, however, it creates surface waves on the top side of the disk. This wave can reach the antenna by propagating horizontally. As a result, the performance of this method didn't meet the intended purpose.

The ground-plane can still be useful as long as we can eliminate the surface wave, hence, the choke-ring antenna was developed. This antenna consists of a circular shaped ground-plane and a series of concentric circular grooves with quarter wavelength depth. These grooves are placed on top of the ground-plane, and are shorted at the bottom and open at the top. These troughs exhibit a very high impedance at the GPS signal frequencies and prevent the horizontal surface waves from forming. As a result, the antenna can be shielded from multipath signals from below and from near horizontal directions by providing a steep cutoff of gain at low elevation angles, while maintaining a high ratio of RCP gain (direct signal) to LCP gain (reflected signal) [Young *et al.*, 1988].

One of the disadvantages of the choke-ring antenna is that the antenna tends to be bulky and heavy. Furthermore, the choke-ring still cannot effectively mitigate multipath signals arriving from high elevation angle (the multipath due to reflections from objects above the antenna). In general, however, choke-ring antennas performed very well in surveying where the dominant multipath sources are ground bounces.

1.2.1.4. Other multipath-rejecting antennas:

Most of the existing multipath-rejecting antennas tend to be bulky and heavy due to the size of its ground plane. Depending on the geographic location of the antenna, this large ground plane can be loaded with wind and/or accumulate snow. Thus, a GPS antenna which can maintain high multipath-rejection and phase-center stability without a ground-plane is desirable. Such antennas, designed by *Counselman* [1999], are compact, lightweight, dual-band, with no ground-plane, and have good multipath rejection. One of these antennas was field tested and has a vertical array of three discrete elements within its vertical radome. Thus, the antenna looks like a vertical post rather than a horizontal platter. The identical array elements are spaced uniformly along the ver-

tical axis and excited with different currents. This difference in the current among the elements determines the directive gain pattern of the antenna. By properly designing the array element and the current feeding level, the antenna can be made to be sensitive to the right circular polarized signal from the zenith direction only.

Because the L1 and L2 wavelengths are different, different distances between the array elements are needed for L1 and L2. Therefore, this antenna has separate L1 and L2 array elements which were fed via separate transmission lines. Both the L1 and the L2 arrays are electrically and mechanically symmetrical with respect to a common center which is also the phase center of the antenna. Due to this symmetry the antenna phase center is independent of direction.

1.2.2. Antenna arrays. Multipath can also be mitigated by using several GPS antennas together. When several antennas simultaneously receive a GPS signal, the multipath geometry is different at each different antenna position in space. Thus, each antenna will exhibit different characteristic of the multipath corrupted GPS signal. By using “spatial processing” technique and by simultaneously processing the multipath corrupted GPS signal, we can identify the uncorrupted GPS signal. In a sense, this array functions as a directional antenna which is more sensitive to the direct path GPS signal than to multipath signals arriving from other directions [Ray *et al.*, 1999].

1.2.3. Long-term signal observation. As a GPS satellite moves across the sky, it will change the reflection geometry of the multipath. Thus, if a receiver observes a GPS signal for a long period, we can identify the multipath signature by examining a daily repeated pattern in the received signal.

One of the classic application of this technique to static GPS receivers is to observe the same GPS satellite for several days continuously. Since the geometry between the GPS satellite and a specific receiver reflector location repeats each sidereal day ($23^h 56^m 4^s$), we can identify the multipath signal by looking for repeated patterns in the signal which are advanced by about four minutes each consecutive day [Elósegui *et al.*, 1995; Georgiadou and Kleusberg, 1988].

1.2.4. Using signal-to-noise ratio. This approach uses the fact that both the carrier phase and the signal-to-noise ratio (SNR) are functions of the location and orientation of a reflector. By using the SNR, the GPS signal reflector geometry can be iden-

tified and phase multipath errors can be estimated [Reichert, 2001].

1.3. The Purpose of the Multipath Simulator

The majority of the previous multipath research has focused on mitigating multipath errors. However, in the early design phase of an experiment, it would be desirable to predict hazardous environmental configuration that can cause severe multipath. With this information, we may attempt to modify the structural configuration if possible, or recommend the best antenna type, location, and orientation within the given configuration. In order to accomplish this, a multipath simulator, MUSTARD, has been developed at the Jet Propulsion Laboratory (JPL).

In essence, the simulator traces the signal as it is transmitted by the GPS satellite to a user's receiver accounting for all possible paths the signal can take by reflecting or diffracting from the surrounding surfaces. In order to account for reflection and diffraction, the Geometrical Theory of Diffraction (GTD) is used [Hansen, 1981; James, 1980].

This sets a lower limit of a few wavelengths on the size of the reflecting objects. (In the case of GPS, the wavelengths are 19.0 *cm* and 24.4 *cm* at L1 and L2 frequencies, respectively.) The multipath signals are then added to the direct signal after accounting for the gain of the receiving antenna. The receiver's tracking loop is then simulated and then range and phase multipath error are estimated. This is done for both L1 and L2 frequencies that the GPS operates on.

This multipath simulator gives a realistic estimate of the error introduced by multipath, and helps to find a means of minimizing the effect of multipath. For precise orbit determination, for example, it provides a quantitative estimate of multipath errors and, thus, can be used for testing different ways of processing simulated observables containing multipath errors.

2. GPS Signal Structure and Observables

2.1. GPS Signal Structure

The GPS transmits two RCP signals at L-band frequencies: L1 at 1575.42 *MHz* and L2 at 1227.6 *MHz*. The L2 signal and the in-phase component of the L1 signal are modulated by pseudo-random precision code (P-code) at a frequency of 10.23 *MHz*;

the quadrature component of L1 is modulated by a coarse acquisition (C/A) code at a frequency of 1.023 *MHz*. A properly equipped receiver will detect amplitude, pseudorange¹, and phase measurements for each of the C/A, L1 P-code (P1), and L2 P-code (P2) signals [Spilker, 1980].

Because the characteristics of C/A and P1 multipath errors are very similar, our discussion below is simplified by considering only one of the two signals. Differences between P1 and C/A multipath will be pointed out as they become significant. To that end it is convenient to model the transmitted P1 and P2 signals as the real part of

$$S_i(t_T) = \tilde{A}_i P(t_T) \exp\left(j(\omega_i t_T + \phi_{Ti})\right) \quad (1)$$

where

- t_T = transmitter time
- i = index for L1 and L2, respectively
- \tilde{A}_i = signal amplitude
- P = PRN code
- $\omega_i = 2\pi f_i$, where f_i is the transmitted freq.
- ϕ_{Ti} = transmitter bias between phase and P-code

The equation does not show the Y (encrypted) code, the C/A component, or the data modulation at 50 *bps*. Note that the transmitter oscillator drift term is included in t_T .

2.2. GPS Observables

Due to the dispersive nature of the ionosphere, the L1 and L2 signals travels at two different velocities. Moreover, the group and phase velocities are different for each frequency. Therefore, we can write the received signal as:

$$R_i(t_R) = A_i P(t_R - \tau_i^g) \exp\left(j\omega_i(t_R - \tau_i^p) + \phi_{Ri}\right) \quad (2)$$

where

- t_R = receiver time
- i = the index for L1 and L2, respectively
- A_i = the received signal amplitude
- τ_i^g = pseudorange
- $\tau_i^p = \tau_i^g +$ differential ionospheric effect on phase
- $\phi_{Ri} = \phi_{Ti} +$ bias between carrier and P-code for the receiver

Note that t_R includes the receiver oscillator drift term. Both τ_i^g and τ_i^p include the transmitter and receiver clock biases. A single GPS measurement consists of four observables: two phase measurements for

the L1 and L2 frequencies, $\Phi_i = -\omega_i\tau_i^p + \phi_{Ri}$, with an unknown bias, and two pseudorange measurements, $P_i = c\tau_i^g$. By ignoring terms of order $1/f_i^3$ or higher, these observables can be written in units of distance as:

$$L_1 \equiv -c \frac{\Phi_1}{2\pi f_1} = \rho + n_1\lambda_1 - \frac{q}{f_1^2} + M_{L1} \quad (3)$$

$$L_2 \equiv -c \frac{\Phi_2}{2\pi f_2} = \rho + n_2\lambda_2 - \frac{q}{f_2^2} + M_{L2} \quad (4)$$

$$P_1 = \rho + \frac{q}{f_1^2} + M_{P1} \quad (5)$$

$$P_2 = \rho + \frac{q}{f_2^2} + M_{P2} \quad (6)$$

where ρ is the non-dispersive delay including the geometric delay, tropospheric delay, clock biases, and any other delay that effects all observables similarly; q is a parameter that is proportional to the total electron content (TEC), which is the integrated electron density between the transmitter and the receiver. Other parameters are:

- c = the speed of light
- λ_i = the wavelength for L1 and L2
- n_i = unknown integer of cycles
- q/f_i^2 = ionospheric group delay and phase advance
- M_{Li} = the carrier multipath in range
- M_{Pi} = the code multipath in range

Terms that are part of the observables but not included the equations 3–6 are data noise, phase center variation, higher order ionospheric terms, and a “wind-up” transmitter-receiver geometry dependent term [Wu *et al.*, 1993]. These terms will be assumed to be negligible, or they can be modeled and subtracted out.

Of importance to the subsequent analysis are the ionospheric free linear combinations:

$$\begin{aligned} \left(\frac{f_1^2}{f_1^2 - f_2^2}\right)P_1 - \left(\frac{f_2^2}{f_1^2 - f_2^2}\right)P_2 = \\ \rho + \left(\frac{f_1^2}{f_1^2 - f_2^2}\right)M_{P1} - \left(\frac{f_2^2}{f_1^2 - f_2^2}\right)M_{P2} \end{aligned} \quad (7)$$

$$\begin{aligned} \left(\frac{f_1^2}{f_1^2 - f_2^2}\right)L_1 - \left(\frac{f_2^2}{f_1^2 - f_2^2}\right)L_2 = \\ \rho + \frac{f_1^2 M_{L1} - f_2^2 M_{L2}}{f_1^2 - f_2^2} + \frac{f_1^2 n_1 \lambda_1 - f_2^2 n_2 \lambda_2}{f_1^2 - f_2^2} \end{aligned} \quad (8)$$

and the P-code multipath linear combinations:

$$P_1 - \left(\frac{f_1^2 + f_2^2}{f_1^2 - f_2^2} \right) L_1 + \left(\frac{2f_2^2}{f_1^2 - f_2^2} \right) L_2 = M_{P1} + C_1 \quad (9)$$

$$P_2 - \left(\frac{2f_1^2}{f_1^2 - f_2^2} \right) L_1 + \left(\frac{f_1^2 + f_2^2}{f_1^2 - f_2^2} \right) L_2 = M_{P2} + C_2 \quad (10)$$

where C_1 and C_2 are biases.

In equations 6 and 7, the ionospheric term is removed and one is left with the pseudorange or biased phase plus a linear combination of L1 and L2 multipath. For the GPS f_1 and f_2 frequencies, the coefficients multiplying P1 and P2 in equation 6 are $2.54 \dots$ and $-1.54 \dots$, respectively. This implies that, if P1 and P2 multipath errors are about equal but uncorrelated, the multipath peak-to-peak amplitude is magnified by about a factor of 3 to that of either P1 and P2 alone. A similar analysis applies for the phase linear combination of equation 7.

In the last two linear combinations, the range, clock, and ionospheric terms are removed from the observables, and one is left mainly with the multipath terms of P1 and P2 plus biases. The biases correspond to fixed numbers over an entire track for a give transmitter and receiver pair. In obtaining equations 9 and 10, we also ignore the carrier phase multipath, since it is generally two order of magnitude smaller than the P-code multipath. The constants multiplying L1 and L2 in equations 9 corresponds to $-4.09 \dots$ and $3.09 \dots$, respectively; while those multiplying L1 and L2 in equation 10 are $-5.09 \dots$ and $4.09 \dots$, respectively.

3. Multipath Effect on the GPS Observables

In order to understand the effects of multipath in any given environment, we need to understand how the PRN ranging receivers operate and how multipath distortion results in ranging errors. The receiver's response to multipath can be parameterized by signal amplitude, time delay, phase, and phase rate. Note that all of the parameters are relative to the direct GPS signal. For the following discussion, a stable multipath is assumed and thus the relative phase rate is assumed to be zero.

3.1. Carrier Phase Multipath

In the presence of multipath signals such as de-

picted in figure 1, the total received signal is the superposition of the direct (equation 2) and delayed replicas of the direct. Concentrating on the carrier and ignoring the P-code modulation, we can write the total received signal as (dropping the subscripts in equation 2):

$$R(t) = A \exp(j(\omega t - \omega\tau + \phi)) + \sum_{k=1}^N A_k \exp(j(\omega t - \omega\tau_k + \phi + \phi_k)) \quad (11)$$

where the sum is over all possible multipath signals, and A and A_k are the amplitudes of the direct signal and the multipath signal from point k , respectively. The corresponding time delays are τ and τ_k ; ϕ_k is the additional phase introduced by the multipath signal coming from point k . In order to find the phase error introduced by the extra paths, we factor out the term $A \exp(j(\omega t - \omega\tau + \phi))$, then equation 10 can be written as:

$$R(t) = A \exp(j(\omega t - \omega\tau + \phi)) \left[1 + \sum_{k=1}^N \frac{A_k}{A} \exp(j(\omega\Delta\tau_k + \phi_k)) \right] \quad (12)$$

where $\Delta\tau_k$ is the extra travel time of the multipath signal from point k . Therefore, an extra phase error is given by:

$$\delta\phi = \arctan\left(\frac{\sum_{k=1}^N \frac{A_k}{A} \sin(\omega\Delta\tau_k + \phi_k)}{1 + \sum_{k=1}^N \frac{A_k}{A} \cos(\omega\Delta\tau_k + \phi_k)}\right) \quad (13)$$

In the limit when $A_k/A \ll 1$ for all k 's, we can expand equation 13 as:

$$\delta\phi = \sum_{k=1}^N \frac{A_k}{A} \sin(\omega\Delta\tau_k + \phi_k) \quad (14)$$

The mathematical model for the effects of a single carrier phase multipath from a planar horizontal surface is well described by *Georgiadou and Kleusberg* [1988] and *Elósegui et al.* [1995].

3.2. Code Multipath

In tracking the transmitted GPS code signal, the received signal is correlated with a locally generated replica of the code. The receiver computes the correlation function between the received signal and the internally generated signal at three different modeled delays called “prompt”, “early”, and “late”. The “early” and “late” delays are different from the “prompt” delay by a receiver sampling interval $+S$ and $-S$ ns, respectively. The receiver effectively fits

a equilateral triangle with base length of two chip period, $2T$, on these three points and declares the location of the peak to be the true delay. In the absence of any multipath, the correlation between the received signal and the receiver generated code can be approximated by a equilateral triangle with a peak value of A as shown in figure 2 (thin solid line triangle) and a phase $\exp[i(\phi_m - \phi)]$. τ_m and ϕ_m are the modeled time delay and phase. In the presence of a single multipath signal with an additional time delay of $\Delta\tau_1$, amplitude of A_1 , and phase shift ϕ_1 , the correlation function can be modeled as the sum of the two triangles corresponding to the direct and the multipath signal as shown in figure 2. The presence of multipath signals corrupt the triangular shape.

The mathematical derivation of the multipath induced pseudorange error by using a “discriminator function” can be found in *Braasch* [1996] and *Van Dierendonck et al.* [1992]. Below we derive the pseudorange measurement error for a given multipath amplitude, delay, and phase shift without using the discriminator function. The formulation is different depending on the receiver tracking strategy, and we have used different threshold for the narrow correlation (the sampling interval being larger or smaller than half a chip period). It should be noted that the formulation ignores the effects of finite bandwidth on the shape of the correlation function.

3.2.1. Wide sampling interval. In the case of the sampling intervals longer than half of the chip length ($S > T/2$), the resulting error in the code measurement, $\Delta\tau^g$, induced by the presence of a single multipath is given by one of the following formulas [*Young and Meehan*, 1988]: Region 1 which applies when $\Delta\tau_1 < T - S + \Delta\tau^g$:

$$\Delta\tau^g = \frac{\Delta\tau_1 \frac{A_1}{A} \cos(\omega\Delta\tau_1 + \phi_1)}{1 + \frac{A_1}{A} \cos(\omega\Delta\tau_1 + \phi_1)} \quad (15)$$

Region 2 which applies when $T - S + \Delta\tau^g < \Delta\tau_1 < S + \Delta\tau^g$:

$$\Delta\tau^g = \frac{(T - S + \Delta\tau_1) \frac{A_1}{A} \cos(\omega\Delta\tau_1 + \phi_1)}{2 + \frac{A_1}{A} \cos(\omega\Delta\tau_1 + \phi_1)} \quad (16)$$

Region 3 which applies when $S + \Delta\tau^g < \Delta\tau_1 < T + S + \Delta\tau^g$:

$$\Delta\tau^g = \frac{(T + S - \Delta\tau_1) \frac{A_1}{A} \cos(\omega\Delta\tau_1 + \phi_1)}{2 - \frac{A_1}{A} \cos(\omega\Delta\tau_1 + \phi_1)} \quad (17)$$

Region 4 which applies when $\Delta\tau_1 > T + S$:

$$\Delta\tau^g = 0 \quad (18)$$

Figure 3 shows the P1 pseudorange multipath induced error $\Delta\tau^g$ as a function of the multipath delay $\Delta\tau_1$. Values of $T = 98 \text{ ns}$, $S = 60 \text{ ns}$, and $A_1/A = 0.1$ are used. The envelope of the multipath error can be readily seen in the figure. The upper envelope corresponds to the multipath error which is in phase with the direct signal, while the lower envelope corresponds to the out-of-phase case. The three different slopes of the upper or lower envelopes correspond to the three different regimes of equations 15–17 and they are separated by two thick black lines in the figure for clarity. The asymmetry of the envelope is amplified for higher values of A_1/A .

The C/A pseudorange multipath induced error is also given by equations 15–18 as long as $S > T/2$, where T is a C/A code chip period. This causes the different regimes of equations 15–17 to trigger at different values of $\Delta\tau_1$. Specifically, the C/A code multipath induced error can grow to 10 times larger than the P-code and does not vanish until $\Delta\tau_1 > T + S$. On the other hand, for various reasons it is the region of small multipath delays that is most important for most GPS applications, and in this region the P1 and C/A multipath errors are the same.

3.2.2. Narrow sampling interval. When $S < T/2$, $\Delta\tau_g$ is given by one of the following formulas: Region 1 which applies when $\Delta\tau_1 < S + \Delta\tau^g$:

$$\Delta\tau^g = \frac{\Delta\tau_1 \frac{A_1}{A} \cos(\omega\Delta\tau_1 + \phi_1)}{1 + \frac{A_1}{A} \cos(\omega\Delta\tau_1 + \phi_1)} \quad (19)$$

Region 2 which applies when $S + \Delta\tau^g < \Delta\tau_1 < T - S + \Delta\tau^g$:

$$\Delta\tau^g = S \frac{A_1}{A} \cos(\omega\Delta\tau_1 + \phi_1) \quad (20)$$

Region 3 which applies when $T - S + \Delta\tau^g < \Delta\tau_1 < T + S$:

$$\Delta\tau^g = \frac{(T + S - \Delta\tau_1) \frac{A_1}{A} \cos(\omega\Delta\tau_1 + \phi_1)}{2 - \frac{A_1}{A} \cos(\omega\Delta\tau_1 + \phi_1)} \quad (21)$$

Region 4 which applies when $\Delta\tau_1 > T + S$:

$$\Delta\tau^g = 0 \quad (22)$$

Note that equation 20 is not a function of T , and the boundary values of each region are different.

Figure 4 shows the P1 pseudorange multipath induced error $\Delta\tau^g$ for the $S < T/2$ case. Values of $T = 98 \text{ ns}$, $S = 48 \text{ ns}$, and $A_1/A = 0.1$ are used. A main distinction between the narrow and wide sampling interval is that in the former, the error exhibit a constant peak value in region 2. This becomes clear as we consider the corresponding figure for the

C/A code. Figure 5 was generated using $T = 980 \text{ ns}$, $S = 48 \text{ ns}$, and $A_1/A = 0.1$. Note that the C/A code multipath induced error exhibits a very wide region 2 and does not vanish until $T + S = 1028 \text{ ns}$.

3.2.3. Multipath Induced Bias. When $A_1/A \ll 1$, region 1 translates to $\Delta\tau_1 < T - S$ (wide sampling) and to $\Delta\tau_1 < S$ (narrow sampling). For $S = 60 \text{ ns}$ (wide sampling) and 48 ns (narrow sampling) this translate to $c\Delta\tau_g < 11 \text{ m}$ and $c\Delta\tau_g < 14 \text{ m}$, respectively. These are above the multipath distance that we will deal with in our discussion later. Therefore, equation 15 (which is identical to 19) becomes valid for P1, P2, and C/A code.

In order to understand the effect of the denominator in equation 15, we plot

$$D(x) = \frac{\cos(x)}{1 + \frac{A_1}{A} \cos(x)} \quad (23)$$

versus x for several values of A_1/A . Figure 6 shows that the effect of the denominator is to change the amplitude asymmetrically for in-phase and out-of-phase multipath. For example, if $A_1/A = 0.5$ then the positive peak is reduced to $2/3$ and the negative one to -2 . Note that this will introduce a negative bias when integrating over a complete cycle. Averaging equation 23 over a complete cycle gives

$$\frac{1}{2\pi} \int_0^{2\pi} D(x) dx = \frac{1}{A_1/A} \left(1 - \frac{1}{\sqrt{1 - (A_1/A)^2}} \right) \quad (24)$$

By averaging over N multipath cycles, we get N times the one cycle average. This implies that multipath does not average out and could cause a significant bias when A_1/A is not small. Figure 7 shows a magnified version of region 1 for $A_1/A = 0.5$. When $A_1/A \ll 1$, $\Delta\tau_g$ varies more or less sinusoidally as a function of the multipath delay, and the multipath bias becomes second-order in A_1/A . For small ratios of A_1/A , the multipath bias is approximately, $-1/2 \Delta\tau_1 (A_1/A)^2$.

Setting aside the amplitude scaling effect of the denominator in equation 15, we can concentrate on the numerator part of the equation and use the approximation

$$\Delta\tau^g \simeq \Delta\tau_1 \frac{A_1}{A} \cos(\omega\Delta\tau_1 + \phi_1) \quad (25)$$

In order to understand more the implication of equation 25, we consider an example of a plane reflector as shown in figure 8. In this example, we have

$$\Delta\tau_1 = \frac{L_m}{c} = \frac{2L \sin \theta}{c} \quad (26)$$

where L_m is the extra traveled distance due to mul-

tipath, L is the antenna height, and θ is the satellite elevation angle. Let $\theta = \omega_s t$, where ω_s is the orbital angular frequency of the transmitting satellite as seen by the receiver. By substituting equation 26 in equation 25, we get:

$$\Delta P = 2L \sin(\omega_s t) \frac{A_1}{A} \cos\left(4\pi \frac{L}{\lambda} \sin(\omega_s t) + \phi_1\right) \quad (27)$$

where λ is wavelength of the carrier signal, and ΔP is $c \Delta \tau^g$. Based on equation 27, ΔP is governed by two oscillations: a slow one, ω_s , and a fast one governed by the \cos term in equation 27. In order to quantify this fast oscillation, we expand the \sin term around a reference angle ϕ_r as follows:

$$\sin(\omega_s t) = \sin(\phi_r) + (\omega_s t - \phi_r) \cos(\phi_r) \quad (28)$$

Using this approximation in equation 27, dropping constant phase terms, and keeping the time varying terms, we can get:

$$\Delta P = 2L \sin(\omega_s t) \frac{A_1}{A} \cos\left(4\pi \frac{L}{\lambda} \cos(\phi_r) \omega_s t\right) \quad (29)$$

Since $\omega_s = 2\pi/\tau_s$ where τ_s is the orbital period of the satellite, we can derive from equation 29 that the period for high frequency multipath oscillation is

$$\tau_1 = \frac{\tau_s}{4\pi \frac{L}{\lambda} \cos(\phi_r)} \quad (30)$$

As is evident from equation 30, the multipath oscillation period is proportional to the wavelength. This implies that P1 multipath is oscillating faster than P2.

Using the values of λ_1 and λ_2 , and the average value of $\cos(\phi_r)$ from 0 to $\pi/2$ which is $2/\pi$ in equation 30, we arrive at the simple ‘‘rule of thumb’’: In about one quarter of a GPS satellite’s revolution (i.e. tracking from horizon to zenith), we should count $10L$ fast oscillations for P1 code multipath error and $8L$ fast oscillations for P2 code, respectively, where L is measured in meters. When the receiver is on a low earth orbiter (LEO), ω_s will be mainly determined by the LEO orbital frequency.

Considering the situation of figure 8 with equation 15, we can plot the P1 and P2-code range error due to one multipath source. Figures 9(a) and (b) show multipath error for P1 and P2 for $L = 1$ m case, respectively. These figures clearly show fast 10 and 8 oscillations, respectively.

When the ionospheric free linear combination is considered (equations 6 and 7), then the multipath frequencies cause a beating phenomenon with two main frequencies: $(f_1 + f_2)/2$ and $(f_1 - f_2)/2$. These frequencies correspond to a long (λ_L) and short (λ_S)

wavelengths give by

$$\frac{2}{\lambda_L} = \frac{1}{\lambda_1} - \frac{1}{\lambda_2} \quad (31)$$

and

$$\frac{2}{\lambda_S} = \frac{1}{\lambda_1} + \frac{1}{\lambda_2} \quad (32)$$

Note that these wavelengths are not to be confused with the widely known wide lane and narrow lane wavelengths.

Using λ_1 and λ_2 equal to 0.19 m and 0.24 m , we get λ_L and λ_S equal to 1.8 m and 0.21 m , respectively. We can arrive at a similar rule of thumb for PC measurement: During the time the GPS satellite goes from horizon to overhead, we should count $10L$ fast oscillations and L slow oscillations where L is measured in meters. Figure 9(c) shows multipath error for ionospheric-free PC measurement for $L = 1$ m , and demonstrates 10 fast oscillations and 1 slow oscillation. All three figures show that averaging over one satellite pass does not average to zero.

Equation 30 can also be directly arrived at by noticing that

$$\frac{1}{\tau_1} = \frac{d}{dt} \left(\frac{L_m}{\lambda} \right) \quad (33)$$

and by using equation 28. Equation 33 is intuitively obvious from the following argument. If in one second the extra multipath distance changes by N carrier wavelength, we should expect N oscillations in the P-code delay or the carrier phase measurements. This is true irrespective of the type of the antenna or tracking loop. From this argument, we can conclude that equation 30 is true for flat surfaces for both the P-code and the carrier phase and for all types of receivers. For other types of surfaces, we should apply equation 33 with the appropriate value for L_m . The above description treats the special case of an antenna above a reflecting plane. There are corresponding rule-of-thumb derivations for reflectors and diffractive sources at various angles.

4. Simulator Description

A multipath simulator, MUSTARD, for analyzing the effects of GPS signal multipath was developed at JPL. This software uses a ray-tracing technique to determine the different paths that a GPS transmitted signal can take. The capabilities of the simulator include:

GPS signals: handles both L1 and L2 frequencies; simulates RCP and LCP reflected and diffracted signals; estimates the multipath delay in the pseudorange and phase measurements

Reflection modeling: uses the Geometrical Theory of Diffraction (GTD) to model signal reflection and diffraction from surfaces, edges, and corners; handles simultaneous reflections from many surfaces

Antenna and receiver: simulates the antenna gain pattern for RCP and LCP signals for L1 and L2; simulates a receiver's operations on incoming signals which produce output observables

Surrounding environment modeling: models flat surfaces of arbitrary shape, spheres or sections of spheres (antenna dishes, inside and outside), cylinders or sections of cylinders, conducting or dielectric surfaces

Geometry: models the motion of the GPS transmitters and receivers and their attitudes to derive time series of the multipath error

By analyzing the real GPS data at the Ovro site, Hajj [1990] showed that the MUSTARD could simulate very reasonable multipath errors. The multipath simulator was also used to assess the multipath error for the Geosat Follow-On (GFO) satellite. The multipath errors predicted by the multipath simulator were compared with the real data from an experiment with a GFO satellite mockup. It was shown that the agreement was good in terms of magnitude, rms value, and frequency [Irish *et al.*, 1998].

Modeling the multipath effects can help determine optimum configurations of the surrounding environment as well as predict the errors that the system will experience. Thus, this software is especially useful in the design phase of a flight mission or ground experiments to quantify the effect of the signal multipath for different GPS antenna types and locations.

4.1. Multipath Modeling

The simulator uses simplified model of the real multipath environment where the geometry of the reflecting structures, the transmitting and the receiving antennas is approximated. The multipath environment is generally modeled as a finite number of surfaces whose dimensions, relative locations, and orientations, as well as their electromagnetic properties are specified.

In modeling the reflection and diffraction from each surface, the Geometric Theory of Diffraction (GTD) is used. The details of this theory is worked out for many types of surfaces with differ-

ent shapes and electromagnetic properties [Hansen, 1981; James, 1980]. Below we present some simple examples of how the MUSTARD ray-trace a signal as it reflects from a flat surface with an arbitrary shape and from an edge.

4.2. Reflection from a Flat Surface

When considering specular reflection from flat surfaces, the problem can be simply stated as follows: In a specified reference frame, given a transmitter at location \mathbf{T} , a receiver at location \mathbf{R} , a flat surface with a defined point on the surface at \mathbf{V} , and a unit vector \mathbf{n} normal to the surface as shown in figure 10; we want to find the point of reflection inside the surface, \mathbf{S} , if any. To do this, we extend the finite surface to an infinite one, and given the latter, we can find the mirror image of the receiver $\mathbf{R}_{\text{image}}$ given by:

$$\mathbf{R}_{\text{image}} = \mathbf{R} - 2\mathbf{n} \cdot \mathbf{R} \quad (34)$$

We can draw a line connecting the image point, $\mathbf{R}_{\text{image}}$, and the transmitter. Then, the reflection point on the infinite surface is the intersection point of the line with the infinite plane. If \mathbf{S} is defined as the solution vector of the reflection point, it should satisfy both the infinite surface equation

$$(\mathbf{S} - \mathbf{V}) \cdot \mathbf{n} = 0 \quad (35)$$

and the line equation connecting \mathbf{T} and $\mathbf{R}_{\text{image}}$

$$\mathbf{S} = \mathbf{T} + t (\mathbf{R}_{\text{image}} - \mathbf{T}) \quad (36)$$

where t is a parameter of a value from 0 to 1. The solution of the equations 35 and 36 is

$$\mathbf{S} = \mathbf{T} + \frac{\mathbf{n} \cdot \mathbf{V} - \mathbf{n} \cdot \mathbf{T}}{\mathbf{n} \cdot (\mathbf{R}_{\text{image}} - \mathbf{T})} (\mathbf{R}_{\text{image}} - \mathbf{T}) \quad (37)$$

The corresponding extra path length, L_{mS} , due to specular reflection is then

$$L_{mS} = |\mathbf{T} - \mathbf{S}| + |\mathbf{R} - \mathbf{S}| - |\mathbf{T} - \mathbf{R}| \quad (38)$$

Once the reflection point is determined on the infinite plane, we need to check whether it lies inside or outside of the finite surface. For the case of a polygon, this is best done by drawing a semi-infinite line in the reflection plane, originating at \mathbf{S} and extending to infinity in any direction. If the line intersects the edges of the polygon zero or even number of times, then \mathbf{S} must be outside of the polygon; otherwise, it is inside it. The amplitude, phase, and polarization of the reflected signal is based on the properties of the surface as well as the incident angle, and is determined by matching the boundary conditions at the surface [Heald and Marion, 1995].

Once the point of reflection, \mathbf{S} , is found, the multipath delay due to specular reflection can be computed. For example, consider a simple semi-infinite plane, where a GPS antenna is located at height L from the surface and at distance d from the edge of the plane as shown in figure 11. Then the delay of the specularly reflected signal with respect to the direct is given by:

$$L_{mS} = 2L \sin \theta \quad (39)$$

where θ is the GPS elevation angle from the surface plane. Assuming the surface to be a perfect conductor, then the specularly reflected signal is completely left-hand circularly polarized with the same power as the direct. It is important to note that the received signal strengths differ due to the difference in RCP antenna gain toward the GPS satellite and LCP gain toward the reflecting surface. Given the multipath delay L_{mS} , the multipath code range error can be computed by using either equation 15 or 19.

4.3. Diffraction from an Edge

When an RCP signal diffracts from an edge, it is generally composed of both LCP and RCP signals. The power contained in each of these components depends on the direction of the incident and diffracted angles and is generally inversely proportional to the distance of the diffracting edge to the antenna. For example, considering the same plane in figure 11, the delay of the edge diffracted signal, L_{mD} , with respect to the direct is given by:

$$L_{mD} = \sqrt{L^2 + d^2} - d \cos \theta + L \sin \theta \quad (40)$$

With this multipath delay, the multipath code range error can be computed by using either equation 15 or 19. The effects of the edge on the polarization and the power of the reflected signal are well characterized by *Kouyoumjian and Pathak*, [1974].

4.4. Antenna Gain Pattern

As discussed in section 1.2.1, partial multipath signal rejection can be achieved by properly shaping the antenna gain pattern and polarization. Usually, the antenna gain pattern is shaped in such a way that overall gain, and particularly LCP gain, drop off quickly at low elevation angles so that reflected signals received at very low and negative elevations are significantly attenuated. Signals from lower elevations are more likely to be reflected from a nearby object.

Figure 12 shows an example of a GPS receiv-

ing antenna gain pattern corresponding to a Dorne-Margoline (D-M) antenna. The figure depicts the antenna gain as function of boresight angle for a specific azimuthal angle and for L1, L2, RCP, and LCP. Note that, for example, for satellite at 30° elevation, the L1 multipath rejection is given by the RCP gain toward the satellite (0 dBic) minus the LCP gain toward the reflection at -30° elevation (-27 dBic) for a rejection factor of 27 dB . The multipath simulator can accommodate any particular antenna gain pattern.

4.5. The BSC multipath simulator

There are other multipath simulators and one of them is Basic Scattering Code (BSC) developed by the Ohio State University. This general simulation software also uses the GTD method and analyzes antenna radiation patterns in the presence of signal reflecting structures. *Axelrad et al.* [1999] compared the results from the MUSTARD and BSC on the Geosat Follow-On (GFO) satellite environment and showed that the agreement between the two multipath simulators was generally very good with similar multipath magnitude and consistent multipath patterns.

The BSC models the antenna as though it were transmitting rather than receiving and computes the resulting far field values. For a lossless antenna the transmitting radiation pattern is identical to the receiving pattern. Thus, it is equivalent to evaluating the response of the antenna to a far field transmission. The BSC computes the horizontal and vertically polarized components of the field, which are then combined for total field as a function of incoming signal direction. It can separate the contributions of direct and reflected signals.

Gomez et al. [1995] used the BSC to model the differential carrier phase errors due to multipath. The accuracy of the BSC simulation has been evaluated by using the data collected on the ground in the presence of multipath producing objects, and good agreement was reported. The BSC was also used in GPS flight experiment called GPS Attitude and Navigation Experiment (GANEX) in the Space Shuttle bay [*Gomez and Hwu, 1997*].

For static environment with no moving part (e.g. IGS GPS ground station antennas, a satellite with fixed structures) multipath errors are only a function of the incoming signal direction and the reflecting surfaces's property but not a direct function of time. Thus, the multipath error can be treated as static

antenna phase center variation. By running the code for different azimuth and elevation angles, we can create a multipath error map covering entire field of view. This results in a table of multipath error as a function of the GPS satellite's zenith and azimuth with respect to the antenna boresight. Then, any multipath error can be computed by 2-dimensional linear interpolation of that table.

This concept was first introduced by *Lippincott et al.* [1996] who used the BSC to generate the multipath error polar map covering the entire hemisphere on a spacecraft environment. *Axelrad et al.* [1999] used a similar approach to investigate the multipath error levels for the Ice, Cloud and land Elevation Satellite (ICESat) Observatory and discussed the effect of the multipath error on orbit determination accuracy.

In spite of the appeal of generating a multipath polar map in a static environment, this approach becomes quickly intractable when the receiver environment is non-static. Even though Axelrad et al. [1999] has used multiple polar maps to study a non-static spacecraft environment where one solar panel is moving, it should be clear that such approach becomes increasingly more difficult with several movable surfaces. The difficulties include the overwhelming number of runs needed to cover all possible configurations, discontinuities, and singularities associated with multi-dimensional interpolation, especially around geometrical boundary regions, or when switching from one multipath error map to the next [*Axelrad et al.*, 1999]

On the other hand, by estimating multipath error as a function of time, where both the GPS constellations and the instantaneous environment configuration are specified at that time, the MUSTARD can easily accommodate any non-static environment and does not require numerous runs. Furthermore, the MUSTARD can easily generate a multipath polar map by providing a list of GPS satellite ephemerides corresponding to a desired set of azimuth and elevation angles.

4.6. Limitations of the multipath simulators

The multipath simulators based on GTD technique has been used successfully to predict multipath environment. However, these GTD based simulators have two main limitations due to the basic nature of the method.

First, GTD is an extension of geometrical optics theory where the wavelengths involved are small

compared with the dimensions of interacting objects. Therefore, the method fails to provide accurate results when scattering from small objects is present.

The second limitation of these simulators is that they assume all reflectors are in the far field of the antenna. When an object is in the near field, induced currents can be generated to alter the antenna gain. In this case a more elaborate technique (e.g. finite elements) would be required to account for the coupling of the antenna and its surroundings.

In general, GTD will provide a reasonably accurate multipath estimate, provided that the reflecting surface edge is at least one wavelength long and one wavelength away from the antenna.

5. Application of the Multipath Simulator

By using the GPS multipath simulator, MUSTARD, we can do various tests to reduce the multipath effects. For example, we can try to find the optimal GPS antenna location and attitude, select the best antenna gain pattern, or we can try different data analysis schemes to improve the overall solution from the GPS data.

The MUSTARD has been used in the early design phase of the TOPEX/POSEIDON satellite mission to quantify the effect of signal multipath for different GPS antenna positions, antenna gains, and data analysis techniques. *Hajj* [1990] showed that the multipath effect can be mitigated up to about 20 *db* lower than the direct signal by properly adjusting the on-board GPS antenna height. It has also been used for the assessment of the GPS signal multipath on the SIR-C/X-SAR free flyer environment for the satellite attitude determination using GPS, and showed that the GPS can be used to meet the attitude requirement on SIR-C/X-SAR [*Hajj and Ceva*, 1994].

Recently, the MUSTARD was used to study the Primary Atomic Reference Clock in Space (PARCS) experiment. The purpose of PARCS is demonstrating state-of-the-art atomic clock performance in space. The microgravity environment of space allows significant improvements in clock performance over ground-based clocks, thus opening up potential ultra-precise reference clocks in space. The demonstration will be carried out on the International Space Station (ISS) in year 2005. It will carry a laser cooled precision clock driven by a hydrogen maser [*Wu and Byun*, 2001; *Byun et al.*, 2002]. GPS measurements accurately determine the ISS orbit. The orbit is needed

for the precise determination of the ISS velocity and position in the Earth's gravitational field, in order to correct for the effects of special and general relativity on the PARCS clock behavior. Since the on-board GPS receiver will operate coherently with the PARCS clock, it will also be used to measure the offset of the PARCS clock from various stable ground clocks connected to their own GPS receivers. The GPS antenna will be located at the Japanese Experiment Module (JEM) where the multipath interference is severe (see figure 13). The application of the MUSTARD to the PARCS experiment is described in the following subsections.

5.1. Spacecraft Modeling

ISS is modeled with a circular orbit at 407 *km* altitude. The orbit elements of ISS at an epoch of 1998:09:22 00:00:00 UTC are as shown in table 1.

This orbit was integrated forward over one day and used as the nominal ISS orbit. For the attitude of ISS, we assumed that the spacecraft body-fixed z-axis always points toward Earth center, the y-axis is normal to the orbit plane but opposite to orbit angular momentum vector, and the x-axis completes the right-handed system. The precise GPS orbits and clocks determined by Flinn network on the same day were used [Jefferson *et al.*, 1999]. L1, L2, and ionospheric-free GPS pseudorange and carrier phase data were simulated between the ISS and all visible GPS satellites at 5 minute intervals over one day.

For modeling of the environment of JEM where the flight GPS receiver will be located, simplified models of three major multipath sources were considered as shown in figure 14. They are stationary objects close to the GPS antenna and consist of Pressurized Module (PM), Exposed Facility (EF), and Experiment Logistics Module-Exposed Section (ELM-ES). The dimension and the relative locations of the modules can be found at http://jem.tksc.nasda.go.jp/iss/doc09_e.html as of writing this article.

5.2. Assessing the Multipath Error

For our study the D-M antenna pattern shown in figure 12 was used, assuming azimuthal symmetry. The antenna is assumed to be placed at the center of the EF, but one meter above its top surface. In general, the GPS antenna field of view is limited to some degrees above the horizon to mitigate the multipath effects. However, since the purpose of this article is

to demonstrate the capability of the multipath simulator, we include all GPS satellites down to zero deg elevation. In our simulation, an average of 9 GPS satellites are tracked at each epoch.

Figure 15 shows relative strengths of direct and reflected signals at L1 and L2 frequencies from each modeled surface. The horizontal axis of each plot denotes the angle of the GPS satellites with respect to the antenna boresight. The dark circle marks denote the direct signal strength while the light plus marks denote the reflected signal strength. In constructing these plots only specular reflection is considered which explains the gaps at certain boresight angles. These gaps imply that no specular reflection is possible when the GPS satellite is at that boresight angle range. From this figure, we can see that the major multipath contributors are EF and PM but not ELM. According to figure 12, the antenna has better multipath attenuation characteristics at L1 frequency (solid line) than at L2 (dotted line). Multipath attenuation is the separation between the RCP gain at the boresight angle (direct signal gain), and the LCP gain at $180^\circ -$ boresight angle (reflected signal gain). This is also seen in figure 15. Note that this figure indicates the relative significance of the multipath from each surface.

Figure 16 shows the P1, P2, and PC pseudorange multipath from EF due to signal reflections only for all visible GPS satellites as a function of the GPS elevation angle. Plotting the multipath with respect to the elevation angle rather than time shows the geometric characteristics of the reflecting structure better. This can be beneficial in the early design phase of the spacecraft. The figure shows that multipath due to signal reflection from EF are mainly from the satellites at high elevation angles. This is contrary to the general notion, but is explained by examining figure 15 and equation 15. Figure 15 shows the ratio of direct to multipath gain is greater toward the antenna boresight. In addition, equation 15 shows the multipath error is proportional to the multipath additional delay, which is $2L \sin(\theta)$ where θ is the GPS elevation angle, so is smaller at low elevation angles. Because of the worse L2-LCP antenna gain pattern relative to the L1-RCP (see figure 12), the P2 signal has larger multipath errors than P1. PC has the highest multipath effect due to the multiplicative coefficients in equation 6.

Figure 17 shows the P1, P2, and PC pseudorange multipath from EF due to both signal reflection and diffraction from all visible GPS satellites. Due

to the small size of EF, the signal diffraction from the edge at low elevation can easily reach the antenna. By comparing figures 16 and 17, it can be seen that the major multipath contribution is from signal diffraction at low elevation angles, and from signal reflection at high elevation angles. Even though not shown, very similar characteristics for phase multipath can be seen but at 100 times smaller scale.

Figure 18 and 19 show the P-code pseudorange multipaths due to reflection and diffraction from ELM and PM, respectively.

As can be seen in figure 15, ELM does not contribute much to the specular multipath error but has a significant contribution to multipath at all GPS elevations when diffraction is included. In the case of PM, a large portion of multipath errors are caused by the signals from the GPS satellites at very low elevation angles due to its vertical reflecting surface.

Finally, figure 20 shows the total P-code pseudorange multipath from all structures; figure 21 shows the total phase multipath from all structures.

Note that in figures 20 and 21, the horizontal axes are a time scale instead of GPS elevation angle. The root sum square value of multipath is 0.71 m for PC, and 0.87 cm for LC as shown in table 2.

5.3. Optimal Location of the Antenna

The effects of multipath on GPS measurements will depend on the antenna location with respect to the reflecting surfaces. When changing the surrounding environment is not an option, a simple approach to reducing multipath is to find the best antenna location within a given environment.

Since the purpose of this article is to demonstrate the capability of the MUSTARD, no extensive search for the best antenna location was performed. Instead, the antenna location was fixed at the center of EF, but its height was adjusted to illustrate the resulting multipath error variation. Table 2 shows the GPS antenna height effect on the multipath error. As the antenna height gets higher, the multipath errors are diminished. The MUSTARD allows the user to choose a height which satisfies a given orbit accuracy requirement. It is probable that better results could be obtained with a more easily accommodated flush-mounted antenna using a more favorably shaped antenna gain pattern.

6. Conclusion

It is possible to investigate the multipath effect

on the GPS signal by using a multipath simulator, MUSTARD, developed at JPL. In essence, this simulator trace the GPS signal as it is transmitted by the GPS satellite to a user's receiver accounting for all possible different paths due to specular reflection and diffraction from surrounding surfaces. In order to account for signal reflection and diffraction, the Geometrical Theory of Diffraction is used. The non-negligible multipath signals are added to the direct GPS signal. The simulator then accounts for the gain of the GPS antennas at L1, L2, RCP, and LCP, and the corresponding induced phase and range errors as measured by a delay-lock loop receiver are estimated.

The multipath simulator can be used in the initial design phase of an experiment to identify environmental configurations that can cause severe multipath. By using the simulator we can also assess the upper limits on the antenna backlobe gains, and be able to determine the ideal antenna location, height, and orientation to minimize the multipath error within a given environment.

Once the optimal geometric configuration is determined, the MUSTARD can provide a realistic and quantitative estimate of multipath errors on GPS data. This in turn can provide a means of testing different ways of analyzing the data to reduce the solution errors from multipath. With a given environment, this simulator is a valuable tool to quantitatively assess the multipath effect on the GPS measurement.

Acknowledgments. The research described in this publication was carried out at the Jet Propulsion Laboratory, California Institute of Technology, under a contract with the National Aeronautics and Space Administration.

Notes

1. Pseudorange is the difference between the transmitter clock at time of transmission and the receiver clock at time of reception. Thus, it is the sum of the actual range between the transmitter and the receiver, atmospheric and ionospheric delays, and transmitter and receiver clock offsets.

References

- Axelrad, P., K. Gold, P. Madhani, and A. Reichert, Analysis of orbit errors induced by multipath for the ICE-Sat observatory, *Proc. of ION GPS-1999 12th International Technical Meeting of The Satellite Division of The Institute of Navigation*, Nashville, TN., Sep.

- 14-17, 1999.
- Bassiri, S., and G. A. Hajj, Higher-order ionospheric effects on the global positioning system observables and means of modeling them, *Manuscripta Geodaetica*, vol. 18, pp. 280–289, 1993.
- Braasch, M., Multipath effects, in *Global Positioning System: Theory and Applications*, vol. I, edited by B. W. Parkinson and J. J. Spilker Jr., Chapter 14, pp. 547–568, AIAA, Washington D.C., 1996.
- Byun, S. H., G. A. Hajj, and L. E. Young, Assessment of GPS signal multipath interference, *Proc. of ION National Technical Meeting*, San Diego, CA., Jan. 28–30, 2002.
- Counselman, C. C. III, Multipath-rejecting GPS antennas, *Proceedings of the IEEE*, vol. 87, no. 1, pp. 86–91, Jan., 1999.
- Elósegui, P., J. L. Davis, R. T. K. Jaldehag, J. M. Johansson, A. E. Niell, and I. I. Shapiro, Geodesy using the Global Positioning System: The effects of signal scattering on estimates of site position, *Journal of Geophysical Research*, vol. 100, no. B7, pp. 9921–9934, 1995.
- Georgiadou, Y., and A. Kleusberg, On carrier phase multipath effects in relative GPS positioning, *Manuscripta Geodaetica*, vol. 13, pp. 172–179, 1988.
- Gomez, S., and S. U. Hwu, Comparison of space shuttle GPS flight data to geometric theory of diffraction predictions, *Proc. of ION GPS-97 10th International Technical Meeting of The Satellite Division of The Institute of Navigation*, Kansas city, MS., Sep. 16–19, 1997.
- Gomez, S., R. Panneton, P. Saunders, S. U. Hwu, and B. Lu, GPS multipath modeling and verification using geometrical theory of diffraction, *Proc. of ION GPS-95 8th International Technical Meeting of The Satellite Division of The Institute of Navigation*, Palm Springs, CA., Sep. 11–15, 1995.
- Hajj, G. A., The Multipath simulator: A tool toward controlling multipath, paper presented at The Second Symposium on GPS Applications in Space, Air Force Geophysics Lab., Hanscom AFB., MA., Oct. 10–11, 1989.
- Hajj, G. A., and J. Ceva, Preliminary assessment of the GPS signal multipath on the SIR-C/X-SAR Free-flyer, JPL Memorandum 335.8-94-008, 1994.
- Hansen, R. C., *Geometric Theory of Diffraction*, IEEE press selected reprint series, IEEE Press, New York, 1981.
- Heald, M. A., and J. B. Marion, *Classical electromagnetic radiation*, 3rd ed., Saunders College Pub., Fort Worth, 1995.
- Irish, K., K. Gold, G. Bonn, A. Reichert, and P. Axelrad, Precision orbit determination for the Geosat Follow-on Satellites, *Journal of Spacecraft and Rockets*, vol. 35, no. 5, pp. 336–341, 1998.

- James, Graeme L., *Geometrical theory of diffraction for electromagnetic waves*, 2nd ed., Peter Peregrinus Ltd., Stevenage, UK., and New York, 1980.
- Jefferson, D. C., Y. Bar-Sever, M. B. Heflin, M. M. Watkins, F. H. Webb, and J. F. Zumberge, JPL IGS analysis center report, 1998 in *International GPS Service for Geodynamics 1998 Technical Reports*, pp. 89–97, Jet Propulsion Laboratory, California Institute of Technology, Pasadena CA., Nov. 1999.
- Kouyoumjian, R. G., and P. Pathak, A uniform geometrical theory of diffraction for an edge in a perfectly conducting surface, *Proc. IEEE*, vol. 62, pp. 1448–1461, Nov. 1974.
- Lippincott, W. L., T. Miliigan, and D. A. Igli, Method for calculating multipath environment and impact on GPS receiver solution accuracy, *Proc. of ION National Technical Meeting*, Santa Monica, CA., Jan. 14-16, 1996.
- Meehan, T., and L. Young, On-receiver signal processing for multipath reduction, *Proc. of the 6th international geodetic symposium on satellite positioning*, Columbus, OH., Mar. 18, 1992.
- Ray, J. K., M. E. Cannon, and P. C. Fenton, Mitigation of static carrier-phase multipath effects using multiple closely spaced antennas, *The Journal of the Institute of Navigation*, vol. 46, no. 3, pp. 193-201, 1999.
- Reichert, A., and P. Axelrad, Carrier-phase multipath corrections for GPS-based satellite attitude determination, *The Journal of the Institute of Navigation*, vol. 48, no. 2, pp. 77–88, 2001.
- Schupler, B. C., R. L. Allshouse, and T. A. Clark, Signal characteristics of GPS user antennas, *The Journal of the Institute of Navigation*, vol. 41, no. 3, pp. 277–295, 1994.
- Spilker, J. J., Signal structure and performance characteristics, in *Global Positioning System*, vol. I, pp. 29–54, The Institute of Navigation, Washington D.C., 1980.
- Stutzman, W. L., and G. A. Thiele, *Antenna Theory and Design*, 2nd ed., John Wiley & Sons, New York, 1997.
- Van Dierendonck, A.J., P. Fenton, and T. Ford, Theory and performance of narrow correlator spacing in a GPS receiver, *Journal of The Institute of Navigation*, vol. 39, no. 3, pp. 265–283, 1992.
- Weill, L., Conquering multipath: The GPS accuracy battle, *GPS World*, pp. 58–66, Apr., 1997.
- Wu, J. T., S. C. Wu, G. A. Hajj, W. I. Bertiger, and S. M. Lichten, Effects of antenna orientation on GPS carrier phase, *Manuscripta Geodaetica*, vol. 18, pp. 91–98, 1993.
- Wu, S. C., and S. H. Byun, Frequency transfer in space with GPS measurements, *Proc. ION GPS-2001. 14th International Technical Meeting of The Satellite Division of The Institute of Navigation*, Salt Lake City, UT., Sep. 11-14, 2001.

Young, L., and T. Meehan, GPS multipath effect on code-using receiver, *Presented at AGU meeting*, Baltimore, MD., May, 1988.

Young, L., T. Meehan, D. Spitzmesser, and J. Tranquilla, GPS antenna selection: Preliminary range and field test results, *Proceedings of ANTEM 88*, Winnipeg, Manitoba, Canada, Aug. 9-12, 1988.

S. H. Byun, G. A. Hajj, and L. E. Young Jet Propulsion Laboratory, California Institute of Technology, 4800 Oak Grove Dr. (Mail Stop 238-600) Pasadena, CA 91109, USA. (Sung.Byun@jpl.nasa.gov; George.Hajj@jpl.nasa.gov; Lawrence.E.Young@jpl.nasa.gov)

(Received _____.)

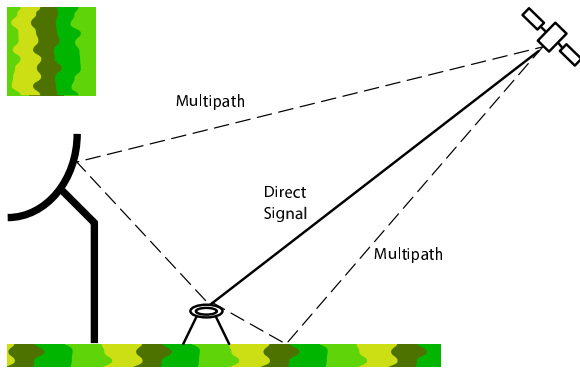


Figure 1. A multipath generating environment

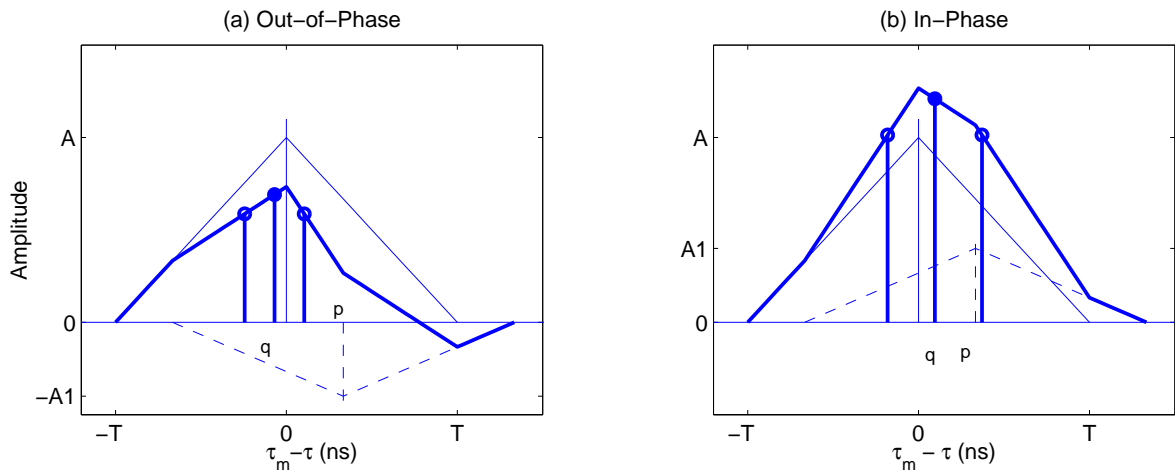


Figure 2. (a) Out-of-phase multipath induced delay. (b) In-phase multipath induced Delay. The thin solid, dotted, and thick solid lines denote the code correlation functions corresponding to the direct, multipath, and the combined signal, respectively. T is a chip period, “ p ” denotes the time delay of multipath signal and “ q ” denotes the multipath induced range error. Note that the resulting multipath induced range error is negative for the out-of-phase case and positive for the in-phase case.

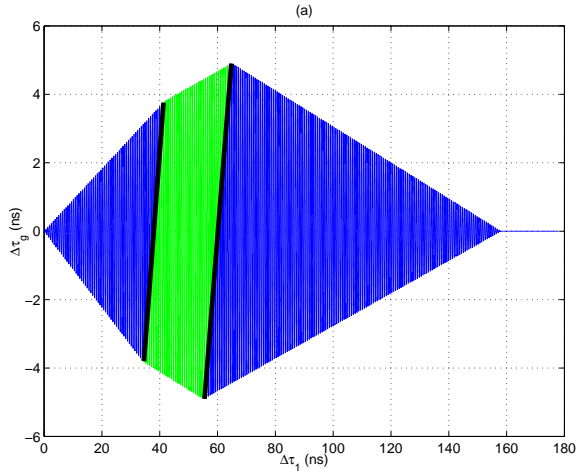


Figure 3. The P1 code tracking error when $S > T/2$ as a function of a single multipath source with multipath delay of $\Delta\tau_1$. The relative multipath amplitude is assumed constant ($A_1/A = 0.1$), values of $T = 98$ ns, $S = 60$ ns, and $\phi_1 = 0$ are used. There are four distinct regions corresponding to equations 15–18. Regions 1–3 are separated by thick solid lines for clarity.

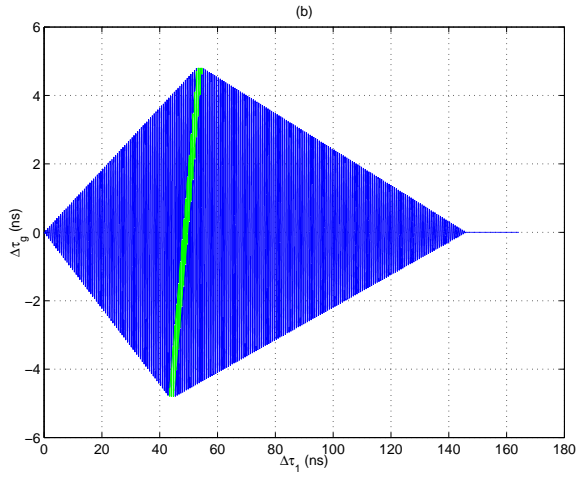


Figure 4. The P1 code tracking error when $S < T/2$ as a function of $\Delta\tau_1$. Values of $A_1/A = 0.1$, $T = 98$ ns, $S = 48$ ns, and $\phi_1 = 0$ are used. The four distinct regions corresponding to equations 19–22.

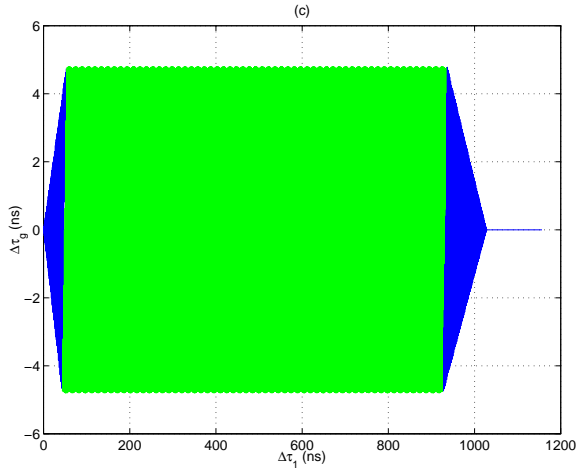


Figure 5. The C/A code tracking error when $S < T/2$ as a function of $\Delta\tau_1$. Values of $A_1/A = 0.5$, $T = 980 \text{ ns}$, $S = 48 \text{ ns}$, and $\phi_1 = 0$ are used. The four distinct regions corresponding to equations 19–22.

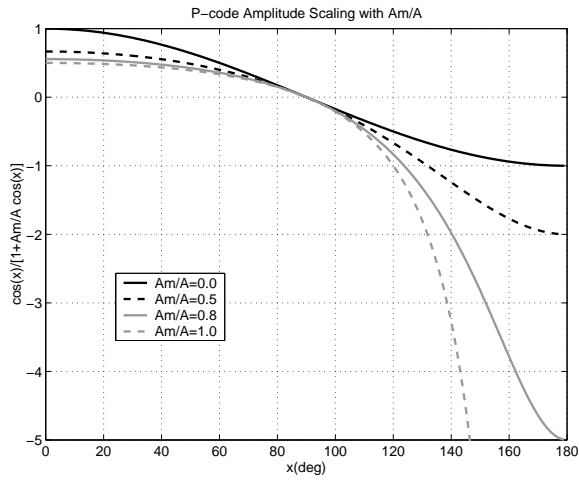


Figure 6. The comparison of P-code tracking error amplitude scaling effect for different values of A_m/A . When $A_m/A \geq 0.5$ a significant bias in the p-code is introduced causing averaging over a complete multipath cycle not to cancel.

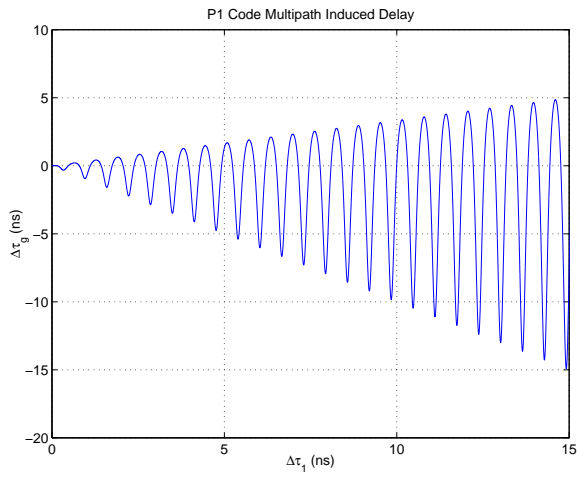


Figure 7. Detailed view of region 1 of the P1 code tracking errors showing the asymmetric and biased oscillation due to the carrier signal. Values of $A_1/A = 0.5$, $T = 98 \text{ ns}$, $S = 48 \text{ ns}$, and $\phi_1 = 0$ are used.

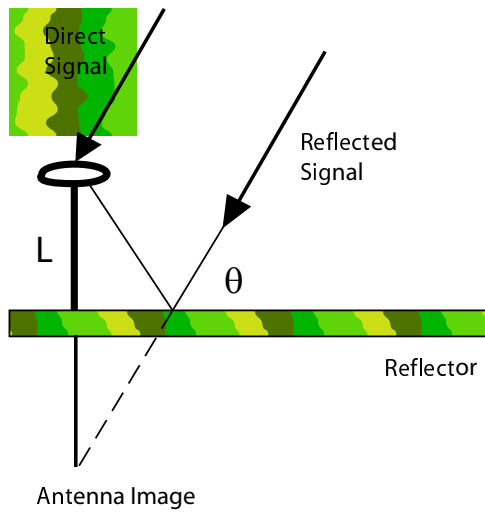


Figure 8. The geometric configuration of an antenna positioned on a planar reflector, the direct and the reflected signal.

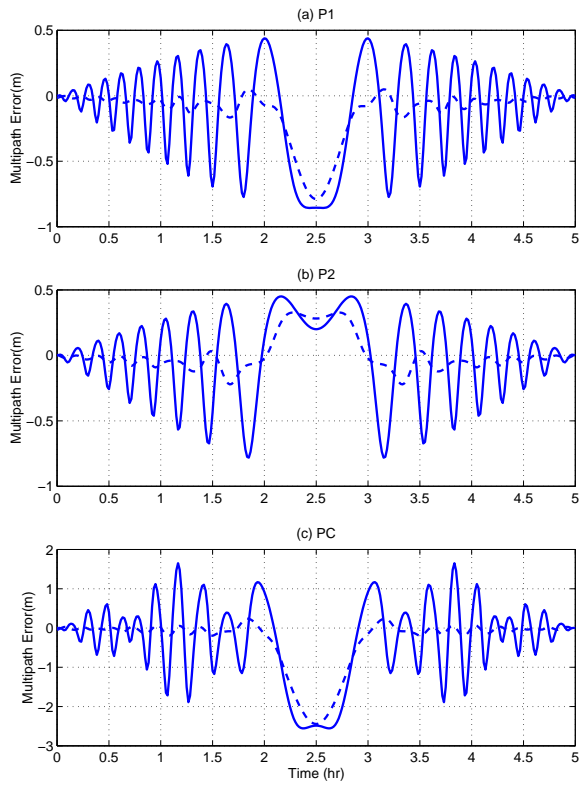


Figure 9. a,b,c, respectively, show P1,P2, and PC multipath errors due to the plane reflector of figure 8 for a GPS satellite going from local horizon to local horizon and passing overhead. The dashed lines show errors after smoothing over 30 mins. During the time the satellite goes from 0–90 degree elevation for an antenna height of 1 m, we count 10 and 8 oscillations for P1 and P2, respectively. For PC, we count 10 fast and 1 slow oscillations.

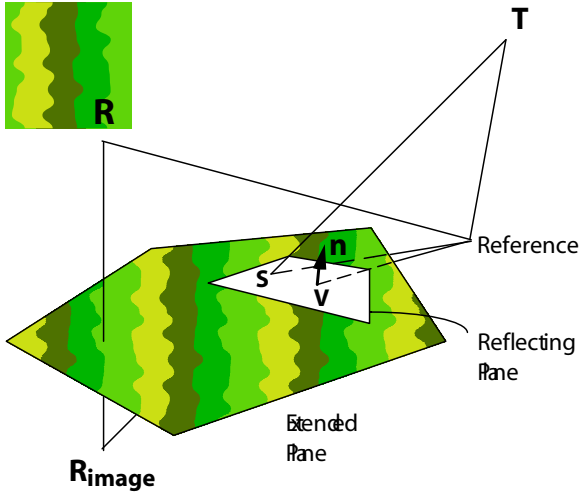


Figure 10. A depiction of specular reflection from a flat surface corresponding to the mathematical description of section 4.2.

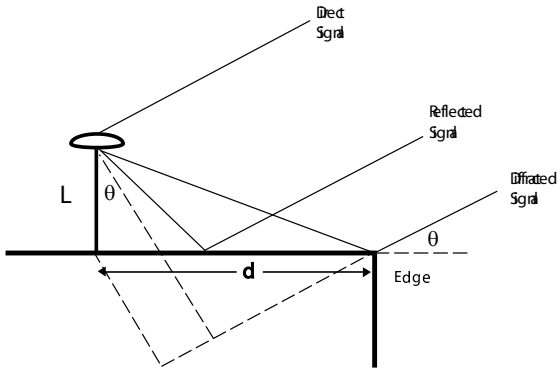


Figure 11. A depiction of reflection and edge diffraction corresponding to equations 39 and 40.

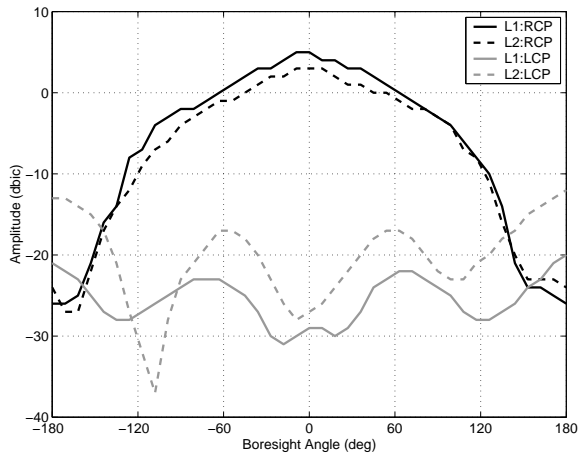


Figure 12. The gain pattern of a Dorne-Margoline antenna. Note that 0 deg corresponds to the antenna boresight direction.

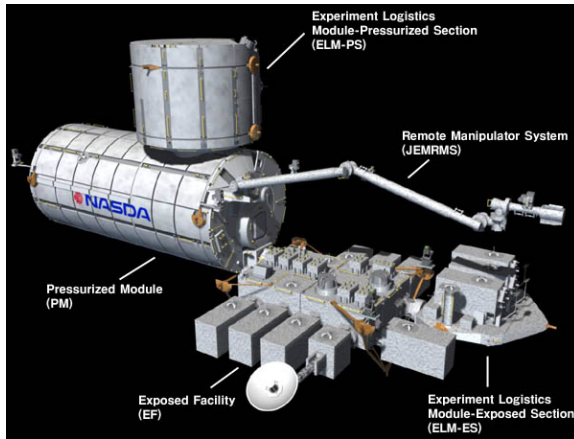


Figure 13. The Japanese Experiment Module (JEM) on International Space Station (ISS).

Table 1. The Orbit Elements of ISS on 1998 09 22, 00:00:00 UTC

Orbit Elements	Data
Semi-major axis	6785 <i>km</i>
Eccentricity	0.02
Inclination	51.6°
Argument of periapsis	90°
Right ascension	330°
Mean anomaly	0°

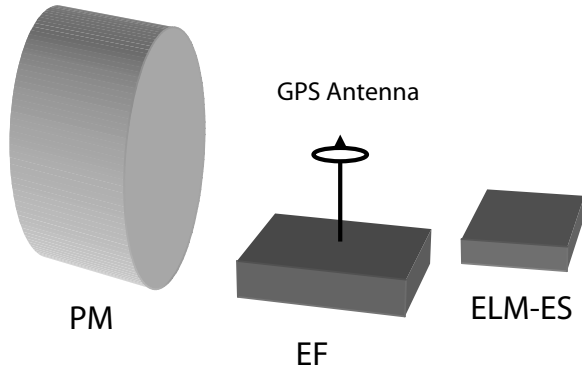


Figure 14. The environmental modeling of reflecting surfaces of JEM showing Pressurized Module (PM), Exposed Facility (EF), and Experiment Logistic Module-Exposed Section (ELM-ES)

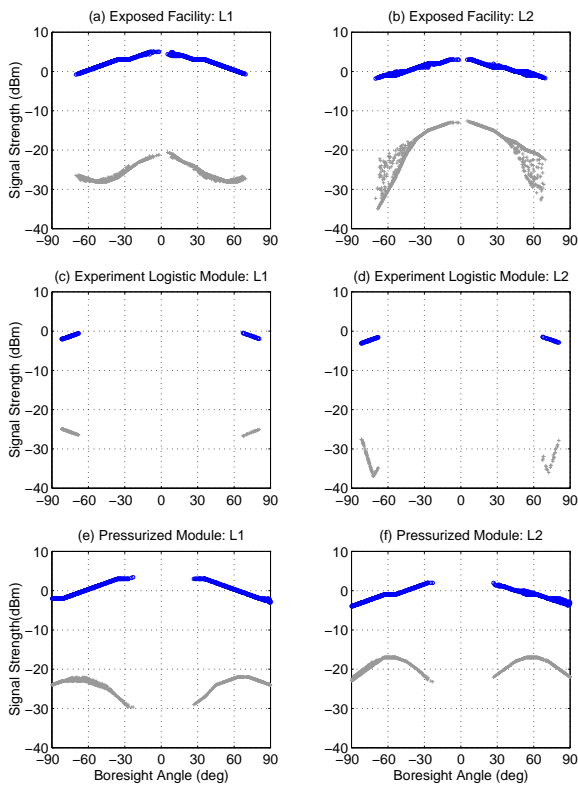


Figure 15. A comparison of the direct (dark color) and specular reflected (light color) signal strength for EF, ELM-ES, and PM structures. Note that 0 deg corresponds to the antenna boresight direction.

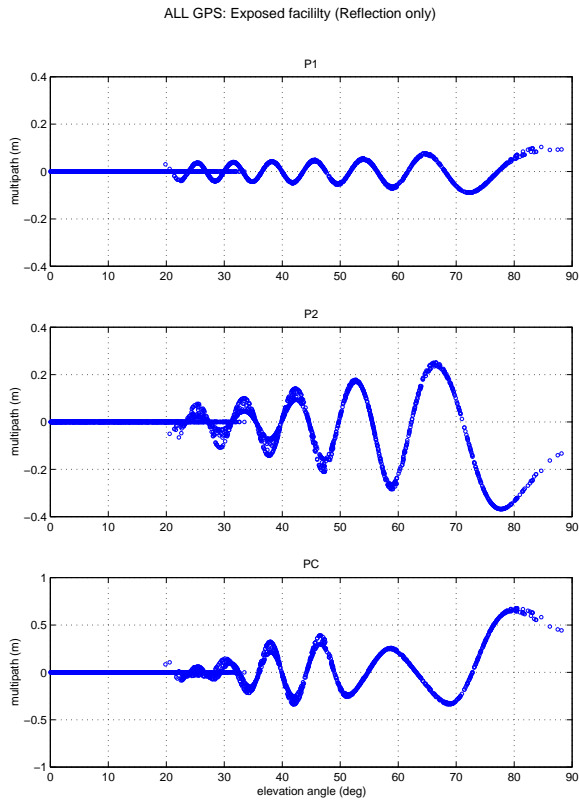


Figure 16. P-code multipath errors due to signal reflections from EF as a function of the GPS satellite elevation angle. Multiple values correspond to different GPS satellites. Zero multipath imply that the satellites are visible (not blocked) but no multipath is present. The simultaneous presence of zero and finite multipath implies that some satellite signals do not experience any multipath while others do.

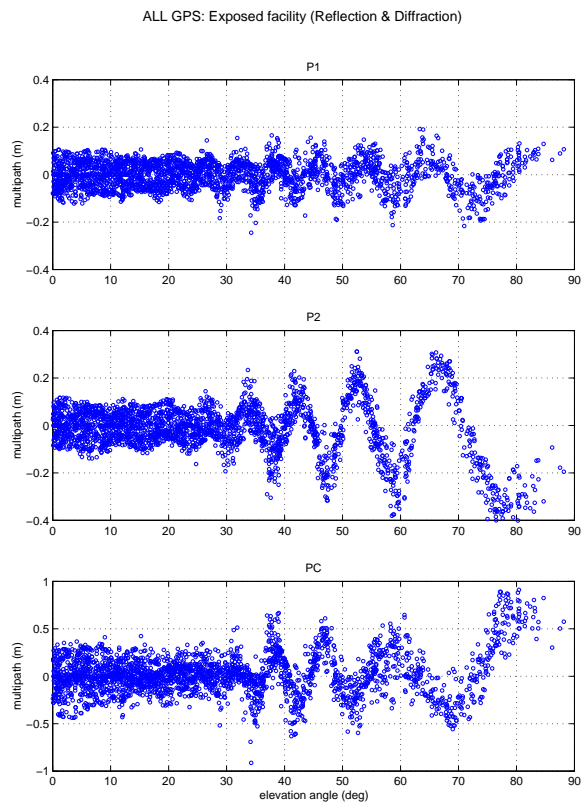


Figure 17. P-code multipath errors due to signal reflections and diffractions from EF as a function of the GPS satellite elevation angle.

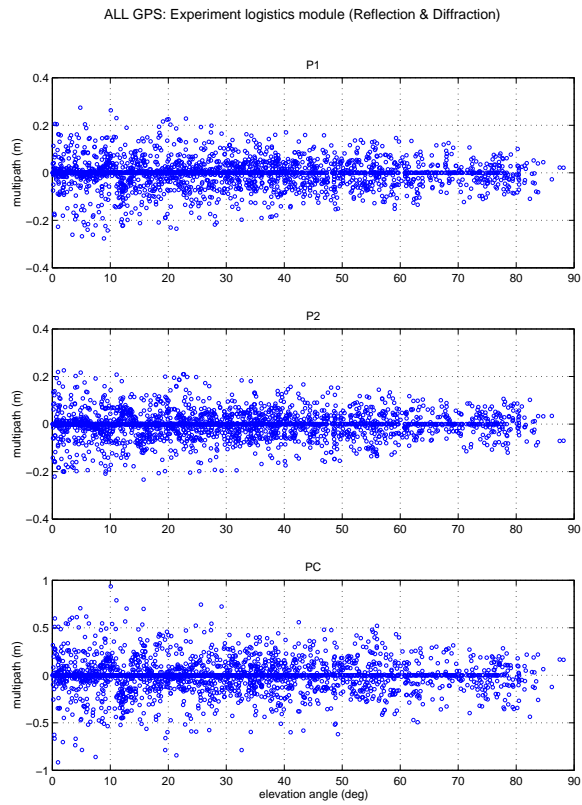


Figure 18. P-code multipath errors due to signal reflections and diffractions from ELM as a function of the GPS satellite elevation angle.

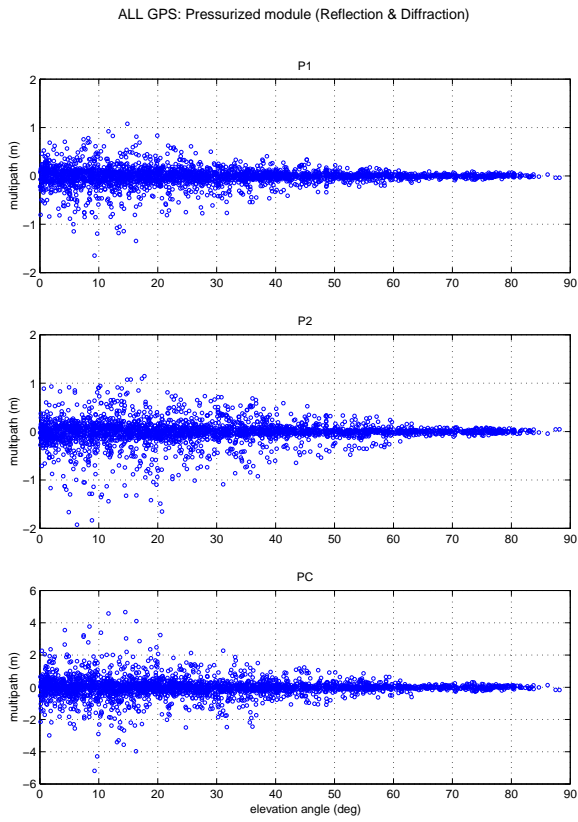


Figure 19. P-code multipath errors due to signal reflections and diffractions from PM as a function of the GPS satellite elevation angle.

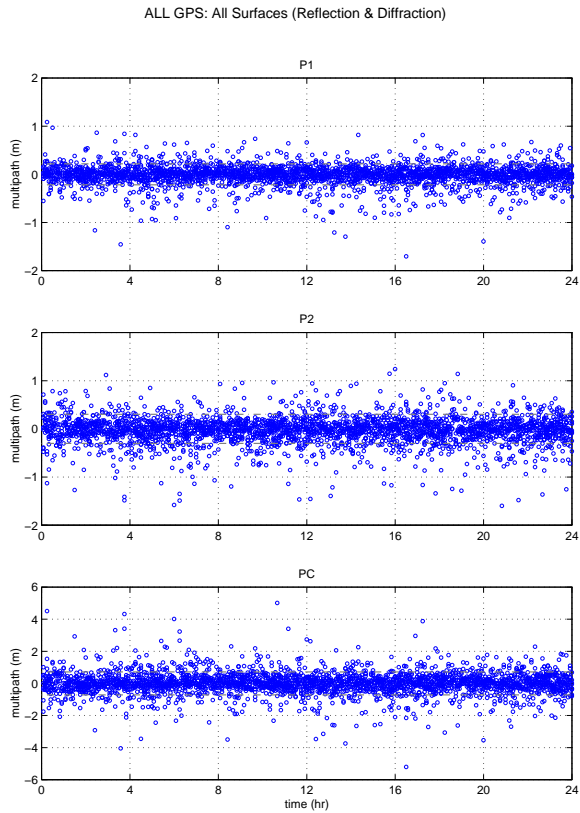


Figure 20. P-code multipath errors due to signal reflections and diffractions from all surfaces with respect to time

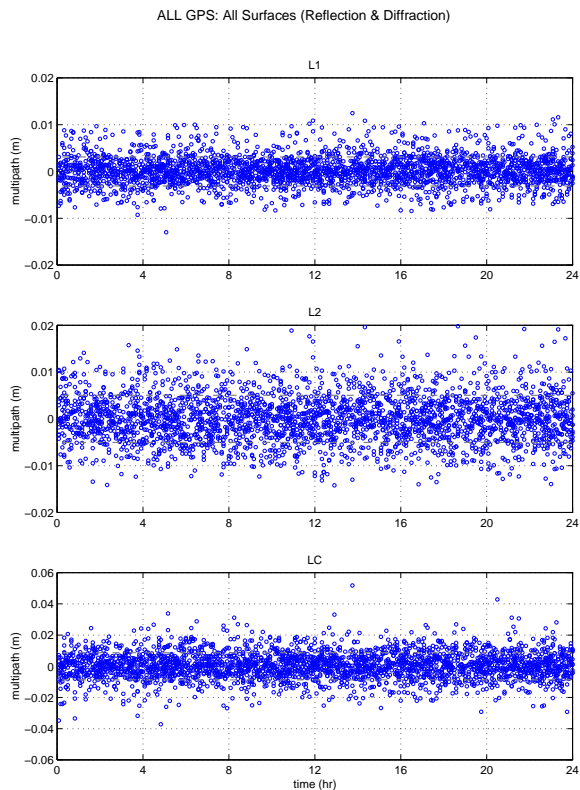


Figure 21. Phase multipath errors due to signal reflections and diffractions from all surfaces with respect to time

Table 2. The GPS Antenna Height Effect on Multipath Error

Ant H	P1(m)	P2(m)	PC(m)	L1(m)	L2(m)	LC(m)
0.2 m	0.2350	0.3345	0.7970	0.0048	0.0068	0.0108
1 m	0.2173	0.3012	0.7137	0.0031	0.0050	0.0087
2 m	0.1889	0.3381	0.7139	0.0028	0.0045	0.0077
3 m	0.1672	0.3591	0.7066	0.0028	0.0044	0.0070
4 m	0.1598	0.3738	0.6759	0.0028	0.0043	0.0067